

Broadband ultraviolet-visible transient absorption spectroscopy in the nanosecond to microsecond time domain with sub-nanosecond time resolution

Bernhard Lang,^{a)} Sandra Mosquera-Vázquez, Dominique Lovy, Peter Sherin,^{b)} Vesna Markovic, and Eric Vauthey^{c)}

Department of Physical Chemistry, University of Geneva, 30 Quai Ernest Ansermet, CH-1211 Geneva 4, Switzerland

(Received 8 April 2013; accepted 18 June 2013; published online 11 July 2013)

A combination of sub-nanosecond photoexcitation and femtosecond supercontinuum probing is used to extend femtosecond transient absorption spectroscopy into the nanosecond to microsecond time domain. Employing a passively Q-switched frequency tripled Nd:YAG laser and determining the jitter of the time delay between excitation and probe pulses with a high resolution time delay counter on a single-shot basis leads to a time resolution of 350 ps in picosecond excitation mode. The time overlap of almost an order of magnitude between fs and sub-ns excitation mode permits to extend ultrafast transient absorption (TA) experiments seamlessly into time ranges traditionally covered by laser flash photolysis. The broadband detection scheme eases the identification of intermediate reaction products which may remain undetected in single-wavelength detection flash photolysis arrangements. Single-shot referencing of the supercontinuum probe with two identical spectrometer/CCD arrangements yields an excellent signal-to-noise ratio for the so far investigated chromophores in short to moderate accumulation times. © 2013 AIP Publishing LLC. [<http://dx.doi.org/10.1063/1.4812705>]

I. INTRODUCTION

Since its invention by Porter and Norrish¹ at the end of the 1940s, flash photolysis has become an essential tool for investigating the mechanism and dynamics of photoinduced processes. Presently, flash photolysis is usually performed with nanosecond excitation pulses produced from a Q-switched laser and probing is achieved either in the kinetic mode, i.e., at a single wavelength with a cw light source and a monochromator equipped with a photodetector connected to a fast oscilloscope, or in the spectroscopic mode using a pulsed Xe lamp and with a gated CCD or diode array detector mounted on a spectrograph. The time resolution is not only determined by the duration of the excitation pulse, typically 5 ns, and by the response time of the detection system, which can in principle be brought below 1 ns, but it also depends on the spectral irradiance (power/area/nm) of the probe light. If the latter is not sufficient, the number of probe photons hitting the detector within a short time interval, e.g., 0.1–1 ns, is too small for a transient change of absorbance of the sample to be detected. In many cases, the spontaneous fluorescence from the photoexcited sample has a larger spectral irradiance than the probe light and, thus, transient absorption changes are totally hidden during the first few tens of nanoseconds after excitation. Such problem does not arise in ultrafast pump-probe transient absorption, where probing is usually achieved with an intense supercontinuum pulse generated by self-phase modulation. Whereas time resolution as short as a few femtoseconds has been demonstrated, conventional pump-probe

transient absorption is limited to maximum time delays of a few nanoseconds. This is essentially due to the necessity to maintain a constant beam profile over the optical delay line which controls the time delay between excitation and probe laser. Riedle and co-workers² could partly overcome this gap using pulsed laser diodes and light emitting diodes (LEDs) for probing. The obtained time resolution is of a few nanoseconds with LEDs and 400 ps with laser diodes. However, the detection in this attempt remains essentially a narrowband technique and beam parameters of LEDs and laser diodes differ to quite some extent from those of a femtosecond supercontinuum. In consequence, difficulties may arise when quantitatively comparing results obtained with nanosecond and femtosecond detection.

Recent developments in the field of short-pulse lasers permit to obtain sufficiently high pulse energies for creating detectable transient absorption changes at rather low costs. The basic idea of the experiment described in this publication is to add an excitation source with pulse duration in the sub-nanosecond domain to an existing ultrafast TA setup and to use the femtosecond supercontinuum as probe in both short pulse and long pulse excitation mode. In the latter, the delay between pump and probe pulses is controlled electronically. Other arrangements have been described where a femtosecond laser system has been electronically synchronized to another ultrafast laser,³ to a synchrotron,^{4–6} or a free electron laser.^{7,8} In contrast to these cost intensive solutions for rather specialized spectral applications, the setup described here employs a passively Q-switched and frequency tripled Nd:YAG laser as excitation source. The time jitter inherent to the passive Q-switching process is measured on a shot-to-shot basis with high accuracy. The obtained time resolution of 350 ps provides a temporal overlap of almost one order of magnitude

^{a)}Electronic mail: Bernhard.Lang@unige.ch

^{b)}Present address: International Tomography Center SB RAS, Institutskaya 3a, 630090 Novosibirsk, Russia.

^{c)}Electronic mail: Eric.Vauthey@unige.ch

between femtosecond (100 fs–2 ns) and sub-nanosecond (350 ps–1 ms) excitation mode. The accessible time scale of an already existing femtosecond TA experiment can thereby be extended into the nanosecond and microsecond time domain without changing the detection system between time scales and on a low-cost basis. The equipment needed in addition to the femtosecond TA setup consists of the excitation source, a high resolution time delay counter, and some diagnosis tools which are commonly to be found in a femtosecond spectroscopy laboratory. The overall costs for the extension amount to less than 10% of the costs of a conventional femtosecond TA setup.

Note that further improving the time resolution of the picosecond excitation mode, e.g., by employing an actively Q-switched and modelocked ps laser as excitation source, would be of no advantage in the arrangement described here since the overlap in time scale with femtosecond excitation is already sufficiently large. The overall signal-to-noise quality is mainly determined by the fluctuations of the femtosecond supercontinuum which is used for detection in both excitation modes. Both excitation modes exhibit therefore signal-to-noise characteristics as they are typical to be found in femtosecond transient absorption spectroscopy experiments. At present, the resulting photometric resolution is of the order of one to a few mOD depending on time binning in picosecond excitation mode. By optimising continuum generation and pixel-to-pixel match between signal and reference CCD camera, there should be still an order of magnitude in photometric resolution to be gained.⁹

II. EXPERIMENT

A. Optical setup

Figure 1 gives a schematic overview of the experimental arrangement. The femtosecond excitation part is not shown here for sake of clarity.¹⁰ Pulses from a Ti:Sa oscillator (1, Spectra Physics Tsunami) are amplified in a commercial amplifier (2, Spectra Physics Spitfire). After compression, a train of pulses of 100 fs duration with 1 kHz repetition rate and 1 mJ energy per pulse at 800 nm is obtained. Trigger signals for the amplifier and the experiments are generated by a programmable delay generator (4, Stanford Research Systems,

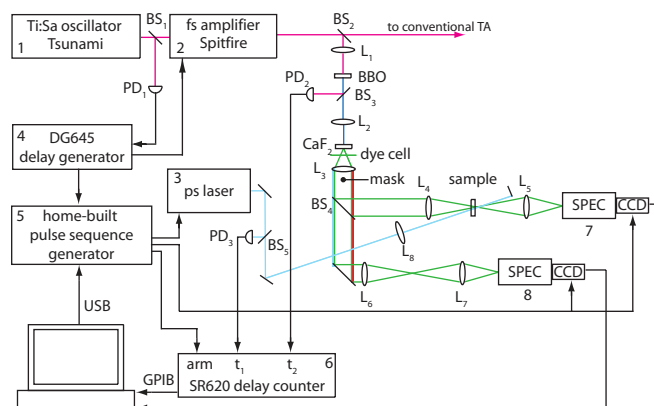


FIG. 1. Schematic drawing of the setup showing only the section with sub-nanosecond excitation.

DG645) using the pulse train of the femtosecond oscillator as master clock which is picked up through a fast photodiode PD₁ (Hamamatsu, S9055) by means of a weak reflection from beam splitter BS₁. About 50 μ J of the amplifier output are branched off (BS₂) and frequency doubled in a β -barium borate (BBO) crystal. The remaining light at the fundamental wavelength is removed by a dichroic mirror (BS₃) and serves through photodiode PD₂ as trigger source for the timing measurement. The 400 nm light is subsequently focused on a 3 mm thick CaF₂ plate using a quartz lens (L₂) with 200 mm focal length to generate a supercontinuum centered at 400 nm. The CaF₂ plate is mounted on two perpendicular translation stages which are continuously moved by two slowly acting DC motors, such that the laser focus scans the plate in Lissajous figures which cover the entire surface, avoiding rapid damage due to color center formation. Note that it is important not to rotate the CaF₂ plate. Though in terms of linear optics CaF₂ is not a birefringent material, its third order susceptibility involved in continuum generation shows anisotropic behaviour.⁹ In femtosecond excitation configuration, another part of the amplifier output can be used for excitation, controlling the time delay between excitation and probe pulse in the conventional way over an optical delay line.¹⁰

Depending on focusing conditions, a continuum generated in the CaF₂ plate extending from 250 nm until the near IR can be obtained.⁹ The strong central wavelength remains well collimated and can be removed by a mask in the center of the white light profile. The spectrum of the continuum is further shaped to a flatter profile in a thin liquid dye cell. A series of achromatic lenses (L₃–L₅) is used to collimate the continuum, to focus it onto the sample cell with a spot size of about 30 μ m, and to refocus it onto the slit of a 1/8 spectrometer (7, Oriel, 77400). The spectra are recorded on a single-shot basis using a high speed full frame CCD chip (Hamamatsu, S7030-0906), digitized and transferred into a PC using PCI burst mode (cameras and PC interface provided by Entwicklungsbüro Stresing, Berlin). Half of the white light is branched off before the sample by a broadband dielectric beamsplitter (BS₄) and sent over an identical pathway (L₆, L₇) into a second spectrometer/camera system (8) for referencing. Thereby, the fluctuations inherent to continuum generation by self-phase modulation are canceled out in the data processing procedure (refer to the Appendix for a more detailed discussion).

The achromatic lenses used in the present setup limit the spectral range of the detection to a lower wavelength of 350 nm. Using quartz lenses on the other hand, we can drive the CCD chips into saturation down to a wavelength of about 280 nm. To make use of the full spectral range without problems due to chromatic aberration in the imaging system, an advanced detection scheme employing all reflective optics in Schwarzschild configuration⁹ is presently being built.

As excitation source for the nano- to microsecond time domain measurements we use a passively Q-switched, frequency tripled Nd:YAG laser (3, Teem photonics, Powerchip NanoUV) which produces a train of pulses at 355 nm with 500 Hz repetition rate, 20 μ J energy per pulse, and 300 ps duration. The excitation beam is focused using a quartz lens with 150 mm focal length (L₈) to a spot size of about 300 μ m. To

ensure a uniform excitation density over the probed spot, the diameter of the pump beam at the sample is kept substantially larger than the probe beam. The excitation laser is triggered at every other femtosecond laser shot to obtain consecutive pairs of absorption spectra with and without excitation pulse. Noise contributions from sample and excitation laser fluctuations are in general strongly correlated in time, resulting in a well-known $1/f$ characteristics, which is to be found all over in nature and in many technical applications.¹¹ Such contributions are best eliminated at high detection frequencies. Thus, in transient absorption spectroscopy best signal-to-noise ratios are in general obtained when performing data acquisition at the highest possible repetition rate, i.e., half the repetition rate of the laser system. Such a detection mode on single-shot basis is essentially equivalent to a lock-in detection with the modulation frequency being set to half the laser repetition rate and with a gated detection in front of the lock-in processing unit to eliminate contributions beyond the Nyquist frequency. Refer to the Appendix for an outline on how to estimate noise contributions in a TA experiment and why a detection using two detector elements together with alternating pulse sequences is in general superior to a detection which employs only one of both.

B. Timing measurements

In parallel to the CCD readout, a high precision time delay counter (6, Stanford Research Systems, SR620) records the time delay between the pulses issued by the two lasers and detects thereby the intrinsic jitter of the passive Q-switching process. Instead of controlling the time delay between the two lasers—which is the cost intensive part of the before mentioned arrangements—we measure the time delay for each pair of pulses and sort the incoming single-shot TA data accordingly. The necessary timing signals are provided by two Si PIN photodiodes (PD₂ and PD₃, Hamamatsu, S9055), which are placed in weak reflections of the femtosecond, respectively, picosecond laser beam. Both diodes are operated with 9 V reversed bias from a battery with a ceramic 100 nF capacitor in parallel to maintain highest possible bandwidth of the response of the diode. The capacitor is directly soldered to the diode with shortest possible wiring to the battery inside a metallic housing which is isolated from the optical table to avoid ground loops. The master trigger from the femtosecond laser system is used for triggering the CCD camera readout and—delayed and divided by two—for triggering the picosecond laser. The latter needs a trigger signal about 60 μ s before issuing a light pulse. To be able to use the full time span of 1 ms between two consecutive probe pulses from the femtosecond system, the trigger pulse for the picosecond system corresponding to probe pulse n at time t_n has to be generated from the trigger cycle $n - 1$ at time t_{n-1} , i.e., 1 ms earlier. An additional gate pulse instructs the time delay counter which pairs of pulses should be measured. The corresponding electronic pulse sequences are provided by a home-built delay generator (5) based on a complex logic programmable device (CPLD) chip (Lattice, LCMXO2280) with a 25 MHz quartz time base which is multiplied to 200 MHz using an internal phase-locked loop circuit. Note that the time resolution

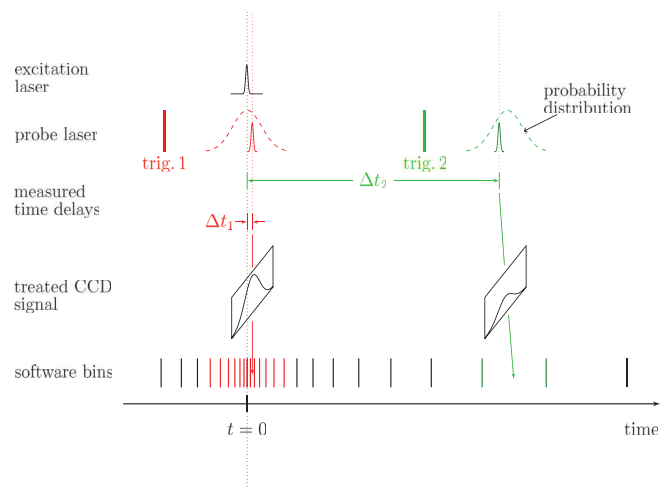


FIG. 2. Timing of the experiment. The two colors correspond to two laser shots with different delay settings.

of the experiment is not affected by the fact that the two time bases are not phase-locked, as the time delay counter measures the total resulting jitter. The pulse sequence generator is connected to the computer through a virtual serial port over universal serial bus (USB) and controls also two shutters used for dark signal measurements and for protection of the sample from overexposure. Command interpreter and pulse sequence logic are implemented on the base of a LatticeMico8 virtual processor written in the hardware description language VHDL.

C. Measurement procedure and data treatment

The acquisition procedure consists of a few preparing measurements and a main loop where the TA data are accumulated. Before entering the main part, time-zero between pump and probe pulse is determined electronically to account for drifts and day-to-day changes in level settings of the triggering system. Measuring and readjusting trigger signals is repeated until the delay values for time-zero are obtained with an error smaller than the desired time resolution around time zero. In a second step, the dark signals of the CCD cameras are measured, followed by a measurement of the supercontinuum without the picosecond excitation source. The obtained spectra are used as reference for the quality of the white light spectrum later on.

The central part of the measurement procedure is sketched in Fig. 2. The main loop consists of reading out the CCD cameras and the time delay counter for a given number of consecutive pairs of shots. Each pair contains one spectrum with and one without excitation laser. For sake of simplicity, the latter is not shown in Fig. 2. The obtained data are processed pair by pair and the procedure reiterated until all bins on the time axis have reached the desired minimal number of accumulations. In the evaluation procedure, first the two white light spectra from the reference CCD camera contained in a pair are checked against the earlier recorded reference measurement. If one of the spectra deviates more than a given multiple of the root mean square (RMS) of the reference measurement, the pair is dropped. Likewise, the pair is dropped

when the result from the time interval counter lies outside a given multiple of the RMS of the time jitter of the picosecond laser which has been determined earlier in the time-zero measurement. Only pairs of spectra which pass these two tests are further treated. The transient absorption is calculated pixel wise using Eq. (A3).

The time axis of the experiment is divided in consecutive logarithmically spaced bins. The user can choose the smallest bin spacing around time zero, the largest decade at the negative and the positive end, respectively, and the number of bins per decade. Through the logarithmic time axis, the bin spacing is adapted to the different needed time resolutions on the different parts of the time scale scanned over during an experiment.

III. RESULTS AND DISCUSSION

A. Signal to noise

As benchmark experiments for testing the performance of the arrangement, we have chosen transient absorption measurements of the triplet state of anthracene and dibromoanthracene in solution. The excited-state absorption bands and the photophysics of these two molecules are well known. They have a sufficiently high molar extinction coefficient at the wavelength of the pump laser of 355 nm and an efficient inter-system crossing from the S_1 to the triplet state. The triplet states of both molecules exhibit a strong excited state absorption around 430 nm which cover the central re-

gion of the supercontinuum used for probing. Figure 3 shows a 3D plot of a TA measurement on dibromoanthracene in acetonitrile. The strong signal centered at 425 nm is due to the absorption of the triplet state which is populated through efficient inter-system crossing upon optical $S_1 \leftarrow S_0$ excitation at 355 nm. In benzene, the lifetime of this state is reported to be 36 μs .¹² However, the samples used for the verification measurements in this work were prepared without purification and deoxygenation. Hence, a substantially shortened lifetime of the triplet state due to quenching by impurities and oxygen is to be expected.

The accumulation parameters for this measurement were set to a resolution of 10 ns around time zero and at least 250 accumulated spectra per bin. The relative noise amounts to about 3% in a single TA spectrum between -100 ns and $+100$ ns. Elsewhere the relative noise is less than 1%. The non-constant noise characteristics are due to the employed acquisition method with logarithmically spaced accumulation bins on the time axis. The 2 μs temporal jitter of the excitation laser acts like a random distribution which is essentially flat over a few hundreds of nanoseconds when sampling the kinetics in a Monte Carlo like procedure around time zero. While waiting for the closely spaced bins in the vicinity of time zero to become sufficiently filled, the remainder of the 2 μs spread also fills up the less densely spaced bins further away to accumulation numbers way beyond the required minimum. Thus, within the interval of ± 1 μs around time zero the signal-to-noise ratio improves the fastest towards the border of that interval. The necessary accumulation time scales linearly with the total number of bins to be filled with the desired minimal number of acquired spectra. As most of the bins are to be found around time zero, the desired time resolution in that range determines the overall accumulation time. On the kinetics, a noise of about 7% is to be found around time zero with the main source of noise being the fluctuations in the excitation laser and sample fluctuation. Further out the quality is improved due to the before-mentioned reasons. The data presented in Fig. 3 were accumulated in about a quarter of an hour.

Note that the signal-to-noise quality obtained in a single shot spectrum has not yet reached the level which can be achieved in a state-of-the-art femtosecond transient absorption setup. This is mainly due to the not yet optimally matched pixel-to-pixel relation in the two spectrometer/camera systems.⁹ Due to the reasons explained above, this manifests itself most notably around time zero when aiming for ultimate time resolution, as demonstrated in the kinetics depicted in the lower panel of Fig. 4. The relative noise on the kinetics amounts here to about 10%. According to our experience with TA spectroscopy using a femtosecond excitation source, we expect that the signal-to-noise ratio can still be improved by at least an order of magnitude so that photometric resolution in the μOD range should be obtainable even at highest time resolution within reasonable acquisition times.

It should also be noted that under long accumulation times, the sample composition may change due to photodegradation. In such case, one may observe additional transient signals with feigned “kinetics” which display the accumulation of the photoproduct during the measurement rather

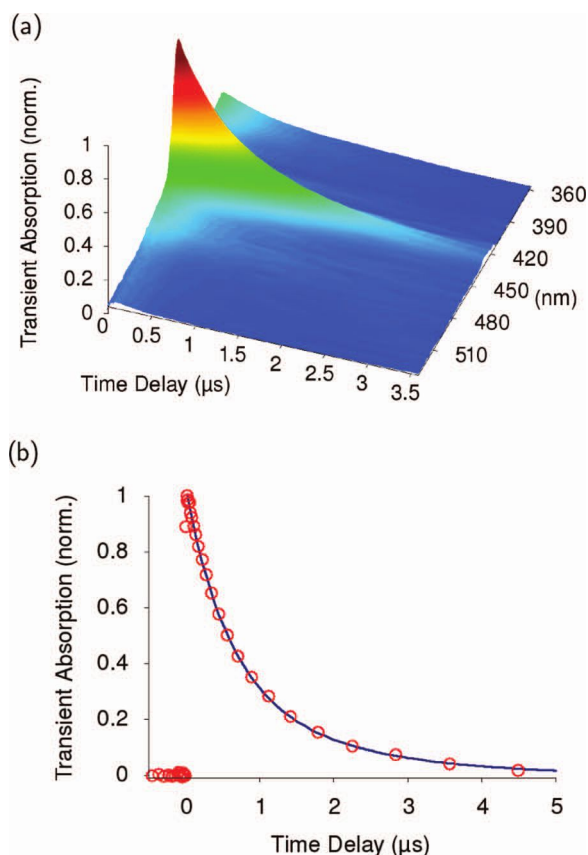


FIG. 3. (a) Transient absorption of the triplet state of dibromoanthracene in acetonitrile, (b) kinetics at the maximum of the band at 425 nm.

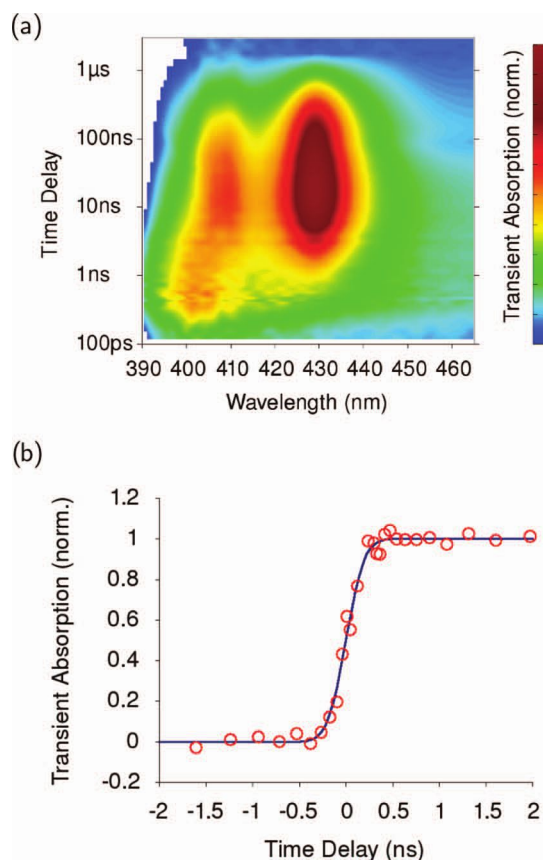


FIG. 4. (a) Transient absorption of the singlet and triplet states of anthracene in acetonitrile, (b) kinetics at the maximum of the singlet excited state absorption at 400 nm around time zero.

than the real kinetics of those signals. This is a common problem in pump-probe experiments where the data have to be recorded sequentially, time delay by time delay. However, using an electronically controlled delay, the solution is obvious. In contrast to a mechanical delay line, the electronics do not induce dead time for changing. It is therefore possible to rapidly scan over the entire delay range of interest multiple times and to perform a quasi-parallel accumulation on all time delays. Components growing in as a function of accumulation time can then easily be identified and eliminated.

B. Time resolution

To determine the effective time resolution, a sample solution with anthracene in acetonitrile was used. In contrast to dibromoanthracene, the intersystem crossing is slower in anthracene due to the absence of the heavy-atom effect. In consequence, the S_1 state has a sufficiently long lifetime to be clearly observed with the time resolution of the picosecond excitation mode. The rise of the corresponding S_1 excited-state absorption, to be found about 30 nm blue-shifted with respect to the triplet state band, is instantaneous on the time scale of the experiment. Similarly, all spectral dynamics due to solvent reorganisation are well finished within 100 ps. The rise of the S_1 excited state absorption is therefore prompt on this time scale and can be used as internal probe to determine the time resolution of the experiment. Figure 4 shows the corresponding 2D plot and a kinetics extracted at the maximum

of the S_1 excited state absorption at 400 nm. The signal of the band reaches 80% of its maximum amplitude within five steps of 100 ps spacing which corresponds to an effective time resolution of the setup of 350 ps. It is worth mentioning that the transition from the S_1 to the triplet state, which manifests itself in the red shift of the band at 400 nm, to be seen in the 2D representation in Fig. 4(a), demonstrates nicely the importance of the ability to cover the time window of the first few nanoseconds in a contiguous fashion. The band shift by about 10 nm during the first couple of nanoseconds reflects in fact the depopulation of the S_1 state by inter-system crossing into the triplet state and the increase of population of the latter. The two corresponding spectroscopic signatures are strongly overlapping in time and spectrum.

The time resolution of the electronics has been determined independently as follows. Two weak reflections from the 400 nm femtosecond beam were directed into two identical Si photodiodes of the type employed in the setup. Both diodes were first connected to a digital oscilloscope (Tektronix, TD3000, 500 MHz bandwidth) using two identical BNC cables to verify the conditioning of the signals. The light intensity was adjusted such that an optimal signal-to-noise ratio could be obtained without reaching saturation. The temporal delay between the two electric signals was then measured with the time delay counter on a single-shot basis. The total electronic jitter between both signals could be determined to $\sigma = 70$ ps RMS with a Gaussian shape. This corresponds to a contribution of $\sigma = 50$ ps RMS from a single diode. Hence, the instrument response function of the electronics is represented by a Gaussian function with 70 ps full-width at half-maximum. This finding was cross-checked using a 80 GHz digital oscilloscope (Lecroy) instead of the time delay counter. With the two diodes, the same result as before was obtained. Using two silicon photomultipliers (Hamamatsu, MPPC S10931-025P) with incident intensities in the strong pile-up range, a pulse-to-pulse jitter of $\sigma = 7$ ps RMS was found¹³ which shows that the 70 ps instrument response is due to the diodes, not the subsequent electronics. The electronic measurement of the time delay contributes thus with 70 ps to the experiment's total time resolution of 350 ps. Hence, the overall time resolution of the experiment is almost entirely determined by the pulse duration of the excitation laser.

IV. APPLICATION EXAMPLES

In the following, we give a glance on two examples of photophysical processes which can be studied using the setup described here. In general, any process traditionally studied with laser flash photolysis can be monitored, with the benefit of a broadband detection allowing to identify intermediate processes and reaction products which may remain undiscovered when using narrow band detection at selected wavelengths.

A. Electron transfer and triplet recombination

Figure 5 shows a measurement of pyrene (Py) and 5 mM dimethylaniline (DMA) in acetonitrile to demonstrate the

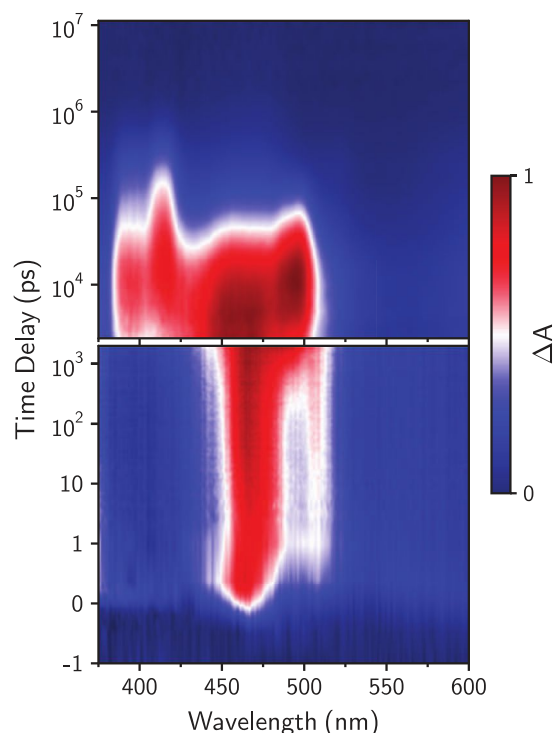
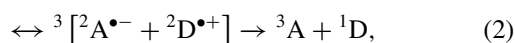
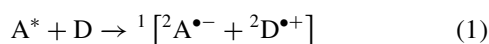


FIG. 5. Transient absorption of pyrene with 5 mM dimethylaniline in acetonitrile. The lower part has been measured using femtosecond excitation, the upper using sub-nanosecond excitation.

capability to extend femtosecond transient absorption measurements into the nano- and microsecond range. The data in the lower half have been obtained with excitation pulses at 320 nm and of 500 fs duration, while for the upper, the picosecond laser in the configuration described in this paper was used for excitation at 355 nm. Upon femtosecond excitation, the band due to the $S_n \leftarrow S_1$ excited state absorption rises within time resolution with a maximum at 460 nm and subsequently red-shifts by about 10 nm due to solvation (dynamic Stokes shift). Some hundreds of picoseconds after photoexcitation, a band growing in at 495 nm and attributed to the $\text{Py}^{\bullet-}$ radical anion indicates quenching of the $\text{Py}^* S_1$ state by electron transfer from DMA. A further band at 420 nm attributed to the Py triplet state is growing in on the timescale of a few nanoseconds. The signal at 400 nm belongs again to the $\text{Py}^{\bullet-}$ signature. As a matter of fact, the signature due to the absorption of $\text{Py}^{\bullet-}$ basically covers the whole range until 380 nm,¹⁴ to which the signatures of the Py S_1 state and the Py T_1 triplet state are superimposed. A decomposition into the different contributions is therefore not straightforward. Note also that the quenching process monitored here is diffusion limited and the kinetics depend thus on concentrations. Altering the concentrations shifts the onsets of the ion and triplet bands to earlier or later times.

Though direct inter-system crossing from the S_1 to the triplet state is also operative, most of the triplet population is generated through triplet recombination of the ion pairs in a reaction scheme as described by



where D and A stand for electron donor and acceptor, respectively. In presence of DMA, the photoexcited S_1 state of Py is quenched by electron transfer, forming a radical ion pair. Due to spin conservation, this pair as a whole is a singlet. In polar solvents, the ions may diffusively separate into free ions or undergo singlet or triplet recombination. The latter case requires first singlet to triplet conversion of the ion pair via hyperfine interaction. Formation of triplet ion pair followed by triplet recombination can also occur upon homogeneous encounter of two ions with parallel spin.¹⁵

B. Magnetic field effect

The experiment described in Sec. IV A was repeated applying a magnetic field of 1330 G to the interaction region. The field was created by two strong permanent magnets attached to both sides of the sample cell using a holder made out of polyoxymethylene (Delrin). Due to the Zeeman effect, the magnetic field lifts the degeneracy of the three triplet levels of the ion pair, leaving only one of them isoenergetic with the singlet state. The triplet recombination pathway is therefore expected to be slowed down in presence of a magnetic field, resulting in an increased signal of the $\text{Py}^{\bullet-}$ radical anion and a decreased yield of the ${}^3\text{Py}$ triplet state.¹⁵ Figure 6 shows the magnetic field effect as a difference spectrum $I_B - I_0$ where I_B denotes the TA signal with and I_0 the TA signal without magnetic field, respectively. Indeed, a considerable increase of the $\text{Py}^{\bullet-}$ radical anion absorption is to be observed. Its spectral signature extends down to about 380 nm, being covered by the stronger $\text{Py}^* S_1$ excited state absorption shown in Fig. 5. At the maximum of the triplet absorption at 412 nm, the decrease of the signal due to the triplet is in fact compensated by the corresponding increase of the underlying $\text{Py}^{\bullet-}$ radical anion absorption, resulting in an almost unchanged transient absorption in this spectral region. To extract the full content of information in these data including the kinetics of the species, one would have to decompose the data into the contributions of three involved species Py^* , $\text{Py}^{\bullet-}$, and ${}^3\text{Py}$, and possibly also a minor contribution from $\text{DMA}^{\bullet+}$, using a combination of time-resolved fluorescence and TA measurements at different concentrations of DMA.¹⁶ Though being a

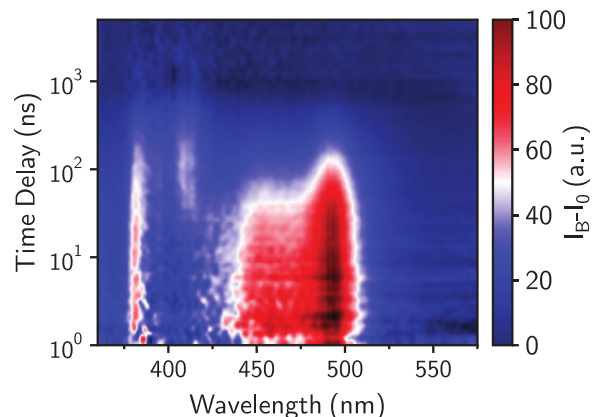


FIG. 6. Magnetic field effect on pyrene with 0.8 mM dimethylaniline in acetonitrile, difference of transient absorption with and without magnetic field.

straightforward procedure, this is beyond the scope of the present publication.

The same donor-acceptor system has been studied by Weller and co-workers¹⁷ in a flash photolysis experiment performed with probe wavelengths of 412 and 470 nm. Applying the same subtraction procedure as described in that publication, we can reproduce the observations for time delays >20 ns. At earlier times the magnetic field effect is more pronounced in our measurements, which could simply be due to the improved time resolution. The experiment was repeated several times and varying the strength of the magnetic field by increasing the distance between the permanent magnets. As soon as the degeneracy of the triplet states is lifted sufficiently beyond an energy difference of kT , the magnetic field effect should not further change. Indeed, no change of the effect was observed when lowering the field to about 600 G, which is in agreement with the saturation plateau starting at ~ 100 – 200 G.¹⁷ On the other hand, the unchanged effect at a lower field strength rules out other artifacts due to the placement of the magnets close to the detection system, since the field attenuation was achieved by changing the geometric positions of the magnets. Further experiments would be needed to clarify the origin of the early-time difference to the findings by Weller.¹⁷ We believe that the increased information content in our broadband data will permit a much more refined spectral decomposition than an analysis using kinetic traces at only two wavelengths.

V. CONCLUSIONS AND OUTLOOK

By combining sub-nanosecond excitation and femtosecond supercontinuum probing, a conventional ultrafast TA setup can be extended to time delays in the nanosecond to microsecond domain without need to change the detection system and at very moderate additional costs. Using a passively Q-switched, frequency tripled Nd:YAG laser and measuring its intrinsic time jitter with a high resolution delay counter, we obtain a time resolution of 350 ps which is essentially determined by the pulse duration of the excitation laser. The thereby given time overlap of almost one order of magnitude between the two excitation modes—using either femtosecond or nanosecond pulses—allows to overcome the gap between femtosecond TA and laser flash photolysis. In contrast to previous approaches using laser diodes as probe, the use of the femtosecond supercontinuum permits a broadband detection which allows the identification of intermediate processes and reaction products which may otherwise remain undetected. A wide variety of photophysical and photochemical processes conventionally addressed with laser flash photolysis can therefore be studied with broadband detection, superior signal to noise quality, and improved time resolution.

At present, an all reflective imaging of the white light path is being built which will extend the spectral range down to 250 nm. Using a Schwarzschild configuration allows to eliminate the astigmatism of the spherical optics and permits a more precised pixel-to-pixel match which will—together with online statistical analysis—bring the noise characteristics of the setup down to the values usually obtained with UV-VIS TA spectrometers. Further spectral extension of the excitation

part is planned. The same type of laser is also available as a frequency doubled Nd:YAG laser with 532 nm and quadrupled with 266 nm wavelength. Both second and third harmonic of the Nd:YAG can easily be reached with the femtosecond excitation by a non-collinear optical parametrical amplifier (NOPA), respectively, by mixing the output of such a device with an 800 nm pulse.

ACKNOWLEDGMENTS

The authors gratefully acknowledge stimulating discussions with and technical help by Benjamin Frisch and Stefan Gundacker from CERN and thank Gerhard Stresing for the helpful assistance in interfacing the CCD cameras, as well as Marcel Dubey, formerly GMP SA, for stimulating the initial idea of the project. We thank Arnulf Rosspeintner for the suggestion of and help with the measurement of the magnetic field effect. We would also like to thank one of the referees for the helpful suggestions to improve the quality of the paper. This work was supported by the Fonds National Suisse de la Recherche Scientifique through Project No. 200020-124393 and the NCCR MUST, and by the University of Geneva.

APPENDIX: CHOICE OF DETECTION MODE

In the following, we outline why in transient absorption measurements the best signal to noise characteristics are in general obtained by recording two separate beams, signal, and reference, together with consecutive pairs of acquisitions, one with and one without sample excitation. Consider the signal S obtained at an arbitrary pixel on the signal CCD camera which monitors the beam transmitted through the sample. According to the Lambert-Beer law, it is given by

$$S = c_S I_0 e^{-(\alpha + \Delta\alpha)} \quad \text{and} \quad S' = c_S I_0' e^{-\alpha'}, \quad (\text{A1})$$

where I_0 is the incident white light intensity before the sample and at the wavelength monitored by the pixel under consideration, α is the steady state absorption of the sample at that wavelength, $\Delta\alpha$ the absorption change induced by the excitation laser, and c_S the conversion coefficient from light intensity to electrical signal of the pixel under consideration. S' is obtained at shots where the excitation laser is off. The primed quantities may have altered since the measurement of S due to fluctuations. For the corresponding pixel on the reference CCD camera, we have

$$R = c_R I_0 \quad \text{and} \quad R' = c_R I_0'. \quad (\text{A2})$$

If the reference beam also passes through the sample, but at a different spot which is not hit by the excitation laser, a factor $\exp(-\alpha^*)$, respectively, $\exp(-\alpha'^*)$ has to be added, where the asterisk denotes that the steady state absorption at that spot may somewhat differ from the excitation spot due to sample fluctuation. From the four recorded signals S , S' , R , and R' , the transient absorption ΔA is calculated as usual by

$$\Delta A = -\log_{10} \left(\frac{S}{R} \cdot \frac{R'}{S'} \right). \quad (\text{A3})$$

To judge the signal-to-noise quality, we have to calculate the shot-to-shot fluctuations $\delta\Delta A$ by error propagation of all

fluctuating quantities

$$\delta^2 \Delta A = \sum_{\xi} \left(\frac{\partial \Delta A}{\partial \xi} \right)^2 (\delta \xi)^2, \quad (\text{A4})$$

where $\delta \xi$ denotes the fluctuation of the quantity ξ . Besides the fluctuations of the excitation and probe laser and the sample, the noise contribution from the data acquisition has also to be taken into account. To this end, we can to first order attribute a zero centered fluctuating contribution to each of the four measured signals (e.g., $S = \langle S \rangle + \delta S$ with $\langle \delta S \rangle = 0$). The terms to be evaluated are thus the derivations of ΔA with respect to $\{\xi\} = \{S, S', R, R', I_0, \alpha, \Delta \alpha\}$. Note that primed and unprimed quantities have first to be taken as independent variables. Only in the final result the primed quantities may be replaced by their unprimed counterparts, making use of the fact that their fluctuations are equal. When using a single detection unit, (A4) evaluates to

$$\delta^2 \Delta A = 2 \left(\frac{\delta^2 I_0}{I_0^2} + \frac{\delta^2 S}{S^2} + \delta^2 \alpha \right) + \delta^2 \Delta \alpha. \quad (\text{A5})$$

The fluctuations of the absorption change $\delta \Delta \alpha$ are induced by the fluctuations of the excitation laser. Possible small correlations to the fluctuation in α are neglected here. For a detection with a second referencing camera with the reference beam not passing through the sample, we obtain

$$\delta^2 \Delta A = 2 \left(\frac{\delta^2 S}{S^2} + \frac{\delta^2 R}{R^2} + \delta^2 \alpha \right) + \delta^2 \Delta \alpha. \quad (\text{A6})$$

In case the reference beam passes through the sample, the last term in the bracket gets augmented by a factor of two, assuming that the sample fluctuations at the two corresponding spots are uncorrelated. Indeed, the dependence on δI_0 to be found in (A5) has disappeared in (A6) which shows that the signal obtained by a two-camera setup does—to first order correlations—depend on probe laser fluctuations.

At first sight, the first two contributions in (A6) seem to suggest that reducing $\delta^2 \Delta A$ is possible by longer integration times, since a longer accumulation increases the denominators of these terms while their counters remain constant. Especially, the relative noise contribution from electronic readout reduces when photons of multiple pulses are integrated on a CCD chip between consecutive readouts. However, the above calculation does not take into account that sample fluctuations, laser fluctuations, and electronic noise contributions are in general strongly correlated in time, leading to a $1/f$ noise characteristic with constant power density on a logarithmic frequency scale. In consequence, the higher the detection frequency, the lower will be the contribution from correlated fluctuations, which is quite obvious for a difference measurement such as transient absorption where data from adjacent points on the time axis contribute to a single acquisition. The further these points are apart in time, the larger is the fluctuation amplitude between them. Note that this consideration

holds also for any other detection scheme where the result is obtained from at least two different signals which for technical or intrinsic reasons cannot be measured at the same time.

The upper limit for the detection frequency is given by the congestion due to readout noise which in general increases with detection frequency due to increased thermal load and poorer counting statistics. Correlated noise decreases with $1/f^\gamma$ with some numeric constant γ depending on the nature of the fluctuation. The relative noise of counting statistics scales with \sqrt{n} where n is the number of detected photons. The characteristics of thermal load strongly depend on the employed acquisition device. At some point in frequency, acquisition noise and counting statistics overcome the suppression of $1/f$ noise and a further increase of the detection frequency will deteriorate the signal-to-noise quality of the obtained data. In a transient absorption measurement which uses as probe a supercontinuum generated with an amplified femtosecond laser source at one to a few kHz repetition rate, the intensity of the probe light is sufficiently strong to make use of the full dynamic range of commonly employed CCD and photodiode array detectors with the light from a single laser shot. The detection frequency of choice is therefore the highest possible, half the laser repetition rate.

¹R. G. W. Norrish and G. Porter, *Nature (London)* **164**, 658 (1949).

²U. Schmidhammer, U. Megerle, S. Lochbrunner, E. Riedle, and J. Karpiuk, *Rev. Sci. Instrum.* **76**, 093111 (2005).

³J. Bredenbeck, J. Helbing, and P. Hamm, *Rev. Sci. Instrum.* **75**, 4462 (2004).

⁴A. A. Zholents and M. S. Zolotarev, *Phys. Rev. Lett.* **76**, 912 (1996).

⁵K. Haldrup, G. Vankó, W. Gawelda, A. Galler, G. Doumy, A. M. March, E. P. Kanter, A. Bordage, A. Dohn, T. B. van Driel, K. S. Kjær, H. T. Lemke, S. E. Canton, J. Uhlig, V. Sundström, L. Young, S. H. Southworth, M. M. Nielsen, and C. Bressler, *J. Phys. Chem. A* **116**, 9878 (2012).

⁶A. M. March, A. Stickrath, G. Doumy, E. P. Krässig, S. H. Southworth, K. Attenkofer, C. A. Kurtz, L. X. Chen, and L. Yough, *Rev. Sci. Instrum.* **82**, 073110 (2011).

⁷S. Schorb, T. Gorkhover, J. P. Cryan, J. M. Glowina, M. R. Bionta, R. N. Coffee, B. Erk, R. Boll, C. Schmidt, D. Rolles, A. Rudenko, A. Rouzee, M. Swiggers, S. Carron, J.-C. Castagna, J. D. Bozek, M. Messerschmidt, W. F. Schlotter, and C. Bostedt, *Appl. Phys. Lett.* **100**, 121107 (2012).

⁸M. Beye, O. Krupin, G. Hays, A. H. Reid, D. Rupp, S. de Jong, S. Lee, W.-S. Lee, Y.-D. Chuang, R. Coffee, J. P. Cryan, J. M. Glowina, A. Föhlich, M. R. Holmes, A. R. Fry, W. E. White, C. Bostedt, A. O. Scherz, H. A. Durr, and W. F. Schlotter, *Appl. Phys. Lett.* **100**, 121108 (2012).

⁹A. L. Dobryakov, S. A. Kovalenko, A. Weigel, J. L. Pérez-Lustres, J. Lange, A. Müller, and N. P. Ernsting, *Rev. Sci. Instrum.* **81**, 113106 (2010).

¹⁰G. Duvanel, N. Banerji, and E. Vauthey, *J. Phys. Chem. A* **111**, 5361 (2007).

¹¹P. Bak, C. Tang, and K. Wiesenfeld, *Phys. Rev. Lett.* **59**, 381 (1987).

¹²S. L. Murov, I. Carmichael, and G. L. Hug, *Handbook of Photochemistry* (Marcel Dekker, Inc., New York, 1993).

¹³S. Gundacker, E. Auffray, N. Di Vara, B. Frisch, H. Hillemanns, P. Jarron, B. Lang, T. Meyer, S. Mosquera-Vázquez, E. Vauthey, and P. Lecoq, *Nucl. Instrum. Methods Phys. Res. A* **718**, 569–572 (2013).

¹⁴T. Shida and S. Iwata, *J. Am. Chem. Soc.* **95**, 3473 (1973).

¹⁵D. R. Kattinig, A. Rosspeintner, and G. Grampp, *Phys. Chem. Chem. Phys.* **13**, 3446 (2011).

¹⁶A. Rosspeintner, G. Angulo, and E. Vauthey, *J. Phys. Chem. A* **116**, 9473–9483 (2012).

¹⁷H.-J. Werner, H. Staerk, and A. Weller, *J. Chem. Phys.* **68**, 2419 (1978).